Graded index confined spin waves in a mixed Bloch-Néel domain wall

D. Osuna Ruiz,* A. P. Hibbins, and F. Y. Ogrin

Department of Physics and Astronomy, University of Exeter, Exeter EX4 4QL, United Kingdom

(Received 25 August 2020; revised 10 December 2020; accepted 11 December 2020; published 28 December 2020)

We propose a mathematical model for describing propagating confined modes in domain walls of intermediate angle α ($0 < \alpha < \pi/2$ radians) between domains. The model is obtained from the linearized Bloch equations of motion and under reasonable assumptions that can apply to the scenario of a thick (80 nm) magnetic patch, which simplifies the calculations without a high impact on the model accuracy. The model shows that there is a clear dependence of the local wave number of the confined spin wave on the local angle of domain magnetization with respect to the wall and on the excitation magnetic field frequency. From this model, we can define a local mode index *in the wall* as a function of such angle and excitation frequency. Therefore, the model can be applied to 1D propagating modes, although it also has physical implications for 2D scenarios where a domain wall merges with a saturated magnetic region. Micromagnetic simulations are in good agreement with the predictions of the model. Our model can also give insight on the effects that curved edge structures may have on the propagating characteristics of spin waves bounded in domain walls.

DOI: 10.1103/PhysRevB.102.224431

I. INTRODUCTION

Due to their low loss and shorter wavelength compared to electromagnetic waves in free space, spin waves are a promising candidate for information carrier in micrometer and submicrometer scale magnonic circuits [1–3]. Inhomogeneities such as vortex cores have been widely studied as spin waves emitters [4–6]. Once the spin wave is excited, an adequate control of its propagation is key for the development of circuits that channel spin waves. Local excitation of spin waves and their spatial confinement have been widely studied in terms of local ferromagnetic resonances due to inhomogeneities [7–9], confinement along edges [10,11], along domain walls, and by domain wall natural fluctuation modes or so-called Winter magnons [10,12]. It is well known that domain walls act as natural channels for spin waves due to the energy well that they present [13]. More importantly, Winter magnons can be excited across a wide range of frequencies since they are gapless modes, which makes them very useful for efficiently directing spin waves in a variety of potential applications.

Graded index media for wave propagation have been widely studied specially in electromagnetics, in the field known as transformation optics [14–16]. The development of structures and metamaterials ranging from nanometer size to centimeters has presented interesting possibilities not exhibited in nature. In addition, graded-index (GRIN) devices, e.g., for optical elements and slow-light devices that may utilize these novel materials, have found application in an extremely wide range of frequencies, from microwaves to visible light.

In the field of magnonics, graded index magnetic media may serve a similar purpose, taking advantage of the high anisotropic behavior of spin waves [7]. For example, tailoring the spin wave propagation in magnetic domains allows the development of lenses for spin waves [17–19]. Regarding unidirectional propagation in domain walls, previous studies have dealt mainly with redirection and steering the spin wave path [20–22], inducing phase changes [23,24] or nonreciprocal paths by means of nonlinear effects [25] or conventional dynamic dipolar interactions [26].

However, anisotropic magnetic media can provide more functionality beyond simply the modification of direction, intensity, or temporal frequency of the spin wave. Spatial frequency modulation or 'spatial chirping' is a widely used technique in telecommunication engineering and photonics. For example, it is used in fiber-Bragg gratings and in other chirped mirrors as filters, where wave number (k) or equivalently wavelength ($\lambda = 2\pi/k$) shows a spatial dependence. The analysis of spatially chirped signals can even be extended to the processing of images where periodic features are visualized in a perspective view. The graded-index technique for steering electromagnetic waves could also have an equivalence for spin waves, and therefore, mathematical tools are required to understand and model this. Using the nonuniform demagnetizing field in a saturated YIG nonellipsoidal rod, the pioneering work from Schlömann [27] for backward volume spin waves and from Stancil [28] for surface spin waves and further experimental results using spatially varying external fields [29] confirmed the realization of the 'spatial chirping' technique for spin waves. A change of wavelength has also been observed by using tapered saturated magnonic waveguides [30].

In this paper, we demonstrate a spatially dependent wave number (spatial dispersion) of confined modes in domain walls (and therefore, in nonsaturated films), providing with an equation that allows us to model their local wave number and propagation properties. We run micromagnetic simulations to

*do278@exeter.ac.uk

model a 'double-teardrop' or 'bowtie' shaped patch, because in remanence it retains a single intermediate domain wall of variable angle between two vortex cores. The results from these simulations show good agreement with the model we propose.

II. DESCRIPTION OF THE MODEL

As a first step to obtain a useful model, and in similarity to what is done in Ref. [23], we search for an expression of a spatially dependent wavelength for a spin wave traveling in a domain wall, based on a Wentzel-Kramers-Brillouin (WKB) approximation [31]. Assuming a Neel-type domain wall along the x direction, this implies that magnetization components at its center can be expressed as: $m_x = m_0 e^{i\omega t}$, $m_y = M_s$, $m_z = m_0 e^{i\omega t} e^{ik(x)x}$. As it will be shown later in this section, this description of the dynamic magnetization is still approximately correct even for a mixed Bloch-Neel wall of an arbitrary angle. Now, let us assume an internal magnetic field perpendicular to the wall and only related to dipolar and exchange interactions, $\mathbf{H}_i = (H_d + H_{ex})\boldsymbol{y}$, where the demagnetizing field is $H_d = H_d(x)$ and the exchange field is $H_{ex} = 2A_{ex}\nabla^2\mathbf{m}(x)/(\mu_0 M_s)$. Substituting $\mathbf{H}_i$ into $d\mathbf{M}(t)/dt = -|\gamma|\mathbf{M}(t) \times \mathbf{H}_i$, we obtain the following expressions for the linearized equations of motion,

$$i\frac{\omega_0}{|\gamma|}m_z = m_x(H_d + H_{ex}) = m_x H_d + \frac{2A_{ex}}{\mu_0 M_s}\frac{\partial^2 m_x}{\partial x^2}, \quad (1)$$

$$\frac{\omega_0}{|\gamma|}m_x = im_z(H_d + H_{ex}) = im_z H_d + i\frac{2A_{ex}}{\mu_0 M_s}\frac{\partial^2 m_z}{\partial x^2}. \quad (2)$$

As in Ref. [23], in order to find an expression for a spatially dependent wave number $k(x)$ that includes the demagnetizing field magnitude $H_d(x) = |\mathbf{H}_d(x)|$, we combine the previous linearized Bloch equations, (1) and (2), by defining a compact expression for magnetization $\phi = m_x + im_z$, assuming $\phi \sim \phi_0 e^{ik(x)x}$. Finally, we can reduce the linearized Bloch equations of motion to the following first-order, complex, nonlinear differential equation (see Supplemental Material [32] for a more detailed derivation),

$$\frac{\omega_0}{|\gamma|} = |H_d(x)| + \frac{2A_{ex}}{\mu_0 M_s}(ixk'' + x^2(k')^2 + 2(x - i)k' + k^2), \quad (3)$$

where ω_0 is the excitation frequency and γ the gyromagnetic ratio and the primes indicate derivation with respect to x. As a first approach to solve this differential equation, we can assume that variations of spin wave wavelength along the domain wall will be smooth, since no sudden changes in the demagnetizing field along the longitudinal direction are expected in a straight domain wall configuration. This can be formulated as $|\nabla H_i| \ll kH_i$ [33] (p. 198). The small variations of the internal field mean in turn that the variations of wave number may be small too, as the ferromagnetic resonance is not strongly changed. Therefore, both variations are assumed to have similar order of magnitude, $|\nabla H_i| \sim |\nabla k|$. The latter two formulated conditions combined suggest that the first and second derivatives of k with respect to x can be reasonably neglected when compared to k^2. Removing the dependences on k' and k'' from Eq. (3) gives an approximate description for

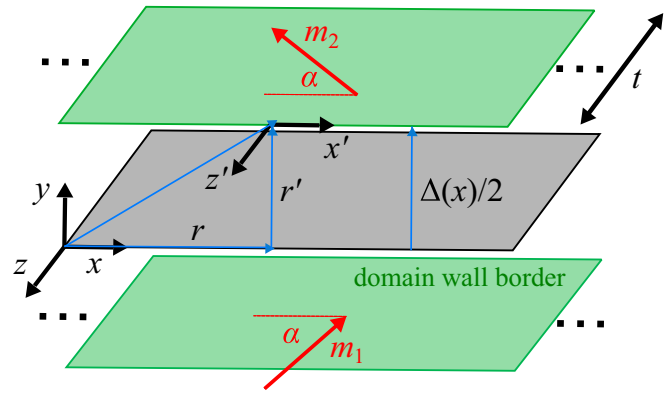

FIG. 1. Schematic of a domain wall in terms of the domain magnetization (red arrows) and their angle (α) with respect to the domain wall of initial width $\Delta(0) = \Delta_0$ in a sample of thickness t. The domain wall borders (green areas) and the domain wall center (black area) are shown. The absolute and relative coordinate systems, chosen for the calculations, are also shown.

a spatially dependent wave number, similar to Schlömann's work [27], as a function of the module of the demagnetizing field in the wall,

$$k(x) = \sqrt{k_0^2 - \frac{\mu_0 M_s}{2A_{ex}}|H_d(x)|}, \quad (4)$$

where $k_0 = \sqrt{\frac{\mu_0 M_s}{2A_{ex}\gamma}}\omega_0$ is the wave number for a confined spin wave of frequency ω_0 when the transversal in-plane demagnetizing field is zero, or in other words, in a 180 degrees Bloch domain wall [25].

Finding a general demagnetizing field expression in a non-saturated ferromagnet of a nonellipsoidal, arbitrary shape is not trivial [34,35]. To do this for our design, we use an approach based on a magnetostatic scenario to find an expression for the in-plane demagnetizing field across the mixed wall, i.e., from one domain into the other. In other words, we aim to establish a link between Eq. (4) and the angle (α) between magnetization in the domains and the wall.

Let us assume the scenario from Fig. 1 for the domain wall of initially constant width $\Delta(x) = \Delta_0$ and an angle α that the magnetization $\boldsymbol{m}_{1,2}$ makes with the straight domain wall. From the pioneering work by Landau and Lifshitz [36], to generally calculate a domain wall structure or profile, the expressions of the specific wall energies involved must be minimized and solved through a method of variational calculus. Examples of this process on standard domain wall types can be found in Ref. [37], Chap. 3.6 and Ref. [38].

Below a critical angle α_c, a mixed Bloch-Neel behavior of the wall is obtained, where the Neel component is always dominant if $t \sim \Delta_0$ or $t < \Delta_0$ and if $\alpha < \alpha_c$ [39]. If $\alpha > \alpha_c$, the out-of-plane component of magnetization in the wall vanishes, and the wall becomes essentially a Neel-type [40]. In Ref. [39], it is found that the critical angle α_c is of $\pi/4$ for a sample as thick as $t \sim 4\Delta_0$. For situations where $t \sim \Delta_0$, the critical angle α_c is almost zero. Therefore, note that the conditions for a dominant Neel component in the mixed wall can be, in principle, easily met in the 80 nm patch modeled

in our work. From micromagnetic simulations (not shown here), the width of the domain wall (as of the vortex core) is approximately ∼90 nm and the domain angles are always smaller than $\pi/4$ radians, yielding in practice a very low critical angle α_c. In addition to this, a $\sin(\alpha)$ coefficient, dependent on the angle of magnetization in the domains, is added to the magnetization in-plane components transverse to the wall (m_y) to consistently model the limiting value before entering into the domains.

Accounting for all the above, following similar calculations to those shown in Ref. [37], Chap. 3.9, and considering that $M_s = \sqrt{m_x^2 + m_y^2 + m_z^2}$ must be satisfied for every y position across the domain wall, the three components of magnetization in the wall region can be regarded as

$$m_x = M_s\sqrt{1 - \sin^2(\alpha)\mathrm{sech}^2\left(\frac{y}{\Delta_0}\right) - \frac{\cos^2(\alpha)\xi(\alpha,y)^2}{(1-\sin(\alpha))^2}}, \quad (5)$$

$$m_y = M_s\sin(\alpha)\mathrm{sech}\left(\frac{y}{\Delta_0}\right), \quad (6)$$

$$m_z = M_s\frac{\cos(\alpha)}{1-\sin(\alpha)}\xi(\alpha,y), \quad (7)$$

where

$$\xi(\alpha,y) = \frac{1+\sin(\alpha)\cosh\left(\cos(\alpha)\frac{y}{\Delta_0}\right)}{\sin(\alpha)+\cosh\left(\cos(\alpha)\frac{y}{\Delta_0}\right)} - \sin(\alpha). \quad (8)$$

A more detailed mathematical description of the derivation of these equations can be found in the Supplemental Material [32]. From Fig. 1, note that $r' = y$. Following an approach based on a magnetostatic scenario and assuming that $\frac{dm_x}{dx} \approx 0$ and $\frac{dm_z}{dz} \approx 0$, a bulk magnetic density charge [$\rho_m(r') = \rho_m(y) = \nabla\mathbf{M}(y) \approx \frac{dm_y}{dy}$] can be found,

$$\rho_m(\mathbf{r}') = \frac{-M_s\sin(\alpha)\tanh\left(\frac{y}{\Delta_0}\right)\mathrm{sech}\left(\frac{y}{\Delta_0}\right)}{\Delta_0}. \quad (9)$$

The antiderivative (i.e., the function resulting from an indefinite integration) of the latter expression [Eq. (9)] effectively retrieves m_y [Eq. (6)]. This expression implies a 'slow' variation of the demagnetising field at the central region of the domain wall ($y \to 0$), in accordance with the y dependence of the 'sech' function. Notice that, if $\alpha = \alpha(x)$, $\Delta_0 = \Delta_0(x)$, and a cross-tie wall were formed, the term $\frac{dm_x}{dx}$ is not necessarily zero, and therefore, it should count into the expression of the bulk magnetic density charge. However, for the sake of simplicity, in this case we consider (i) slow variations of the domain angle, (ii) a constant domain wall's width along its length ($\frac{d\alpha}{dx} \approx 0$ and $\frac{d\Delta_0}{dx} \approx 0$), and (iii) no formation of a cross-tie profile, as we can observe in simulations [see Fig. 3(a)]. Hence, we can assume $\frac{dm_x}{dx} \approx 0$. Also, an 80 nm thick patch is considered, sufficiently thick so that at the central region of the patch, far enough from the surface pinning effects, variations of magnetization across the thickness can also be neglected ($\frac{dm_z}{dz} \approx 0$) even despite the formation of a cross-tie wall [41].

Under the above mentioned assumptions, and due to the conservation of the transverse component of magnetization (m_y) in the domain wall border (following on the schematic from Fig. 1), surface magnetic charges can also be considered negligible ($\sigma_m = m_{y,1} - m_{y,2} = 0$). Choosing the right integration volume, for example a rectangular prism of chosen dimensions equivalent to the domain wall width (Δ_0) in the x and y directions and to the total thickness (t) in the z direction, an expression of the demagnetizing field can be found. The resulting expression, derived from the magnetostatic potential obtained in turn from the defined magnetic density charge, Eq. (9) (see Supplemental Material [32]), is

$$H_d(y) = \frac{-tM_s\sin(\alpha)\tanh\left(\frac{y}{\Delta_0}\right)\mathrm{sech}\left(\frac{y}{\Delta_0}\right)}{4\pi y}, \quad (10)$$

where t is the thickness of the magnetic patch and Δ_0 the 'constant' domain wall width. A more detailed derivation of Eq. (10) is shown in the Supplemental Material [32]. Note that Eq. (10) is only valid for values of y in the wall region ($\frac{-\Delta_0}{2} < y < \frac{\Delta_0}{2}$). The demagnetizing field from Eq. (10) shows an overall even symmetry due to the 'sech(y/Δ_0)' and 'tanh$(y/\Delta_0)/y$' even functions and yields lower demagnetizing field magnitude values at positions off the wall center ($y \neq 0$). This is in good agreement with the observations made in Ref. [42] for a Neel wall. In the latter reference, they suggest that a larger wave number is expected at positions slightly displaced from the wall center because magnetization **M** and wave vector **k** make an angle θ_k smaller than $\pi/2$ radians, due to the turning magnetization in the domain wall structure. Therefore, as the mode there is not in a full Damon-Eshbach configuration, it may show features from the backward volume regime, which for an exchange spin wave implies a larger wave number for the same excitation frequency. Notice that the angle θ_k in Ref. [42] is different from the variable angle α in our model, which indicates the orientation of magnetization in the domains with respect to the direction of the wall. Also, Eq. (10) yields a numerical indeterminate at the center of the wall although this is not a physically realizable solution. At the midwidth (taking the limit $y \to 0$) of the domain wall, where the confinement of the mode is the strongest (in accordance with the maximum of the 'sech' function), and assuming $t \sim \Delta_0$ in a sufficiently thick sample (as assumed above), Eq. (10) finally leads to

$$H_d(\alpha) = \frac{-M_s\sin(\alpha)}{4\pi}. \quad (11)$$

This equation expresses the demagnetizing field perpendicular to the wall at its core in terms of the arbitrary angle of magnetization between the magnetic domains and the wall. Moreover, it is consistent with the assumption of a dominant Neel component in the domain wall profile.

Considering Eq. (11) further, it is worth noting that at an angle of $\alpha = \pi/2$ there is, by definition, no domain wall since magnetization is 'continuous.' The wall width is by definition 'zero,' suggesting that the model no longer applies. The competition between dipolar and exchange energies means that this angle will also determine the width of the domain wall. In other words, finding an expression for the demagnetizing field as a function of the domain angles and the

domain wall width is a self-consistent problem. In order to find a more complete and exact expression for $H_d(x)$, given $\alpha = \alpha(x)$, an additional demagnetizing field should be derived from the respective magnetic potential, obtained in turn from the magnetic density charges defined by $\frac{dm_x}{dx}$ in a similar way. These considerations, together with a variable domain wall width $\Delta(x)$, add more complexity to the model. However, as described before, the following reasonable assumptions can be made for sake of simplicity in our approximate model: (1) Since the maximum intensity of the confined mode will be at the center of the domain wall ($y \to 0$) for the chosen excitation frequencies [22,25,42], the quotient $\frac{y}{\Delta_0}$ is very small regardless of the domain wall width while $\Delta_0 > 0$, or equivalently, for $\alpha < \pi/2$. In fact, it is under these conditions that the proposed model is intended to be applied. Therefore, there is a certain equivalence between $\frac{y}{\Delta_0}$ and y when $y \to 0$, so replacing the first term by simply y in the equations avoids the dependence on the wall width (this can be formulated as $\frac{y}{\Delta_0} := y$). (2) The main assumption for these results is that the demagnetizing field is orientated almost fully in-plane and perpendicular to the domain wall. This assumption is not far from reality, since it has been shown that, in mixed domain walls (between 180 degrees Bloch and Neel wall), the Neel component is dominant. This behavior is observed in arbitrary α-Bloch walls where $\alpha < \pi/2$ radians. In fact, above a critical angle, the out-of-plane component of magnetization vanishes, and the wall becomes essentially a Neel wall [40]. Not only that, this argument is even more convincing for thicker samples since the critical angle reduces with increasing thickness almost reaching zero when $t \sim \Delta_0$ [39]. Equation (11) is consistent with these results, since it also reduces in magnitude as α reduces.

After all these considerations, we need to stress again that finding an exact solution for a local demagnetizing field is very often an extremely complicated task for nonellipsoidal shapes, even in saturation or quasisaturation [35,43,44]. When not found numerically through micromagnetic simulations, approximate analytical approaches are usually taken under reasonable assumptions [34,45]. For all this, and realizing that Eq. (11) is a physically consistent model for the defined scenario, we consider it from now on as a valid first approximation for the transverse demagnetising field along a domain wall of variable domain angle. Therefore, this expression can be combined with Eq. (4) to give the dependence with the variable angle between magnetic domains,

$$k(x) = \sqrt{k_0^2 - \frac{\mu_0 M_s^2}{8\pi A_{ex}} \sin(\alpha(x))}. \tag{12}$$

This equation relies on an initial $\mathbf{k}$ (k_0 $\mathbf{x}$) which is found to be the wave number of a Winter's magnon for a frequency ω_0 through a 180 degrees domain wall (i.e., when $\alpha = 0$). Regarding this, through the dispersion relation of Winter's magnons [$\omega_0(k_0)$], a spatial modal index can be defined as $n(x, \omega_0) = k(x)/k_0$,

$$n(x) = \sqrt{1 - \frac{|\gamma|}{\omega_0}|H_d(x)|} = \sqrt{1 - \frac{\omega_M}{4\pi\omega_0}\sin(\alpha(x))}, \tag{13}$$

where $\omega_M = \gamma M_s$ and ω_0 is the frequency of a continuous wave excitation. This equation predicts the change in wave number (or wavelength) from a given k_0 along the domain wall. In other words, a different initial k_0 will give different values of local wave numbers, but always varying with α in accordance to this model. Therefore, this applies as well to the mode index if we assume an index of unity for an arbitrary initial k_0. Figure 2(a) shows a contour plot of the real values of Eq. (13) as a function of the magnitude of H_d and $f = \omega_0/2\pi$. Most importantly, it shows how at lower frequencies, the change in wave number is more sensitive to the transversal demagnetizing field than at higher frequencies. Figure 2(b) shows the same behavior even when Eq. (11) is introduced into Eq. (13), which reflects now the dependence on the angle α.

It can be inferred from Eq. (13) that, in the absence of a biasing field, there is an upper limit for the frequency at which a mode index of zero can be obtained. This maximum is reached when the demagnetizing field is maximal. In principle, in terms of the magnetic moments' orientation, this is when $\alpha = \pi/2$. However, notice that, in this situation, the definition of domain wall is meaningless. The scenario would imply the vanishing of the domain wall into a saturated region in the y direction (i.e., a magnetic domain). In that region, Eq. (13) can be modified by replacing the formerly dominant demagnetizing field from the (also former) domain wall by an expression of an effective or internal magnetic field H_i. Interestingly, Eq. (13) implies then that a mode index of zero would be obtained at $\omega_0 = |\gamma|H_i$, which is actually the ferromagnetic resonance main mode (i.e., all precessions in phase) of a saturated film for a given internal field H_i. This result agrees with the wave perspective of a uniform ferromagnetic resonance (FMR) precession, which lays a wave number of $k = 0$ (infinite wavelength and $n = 0$). Additional simulations (see Supplemental Material [32]), show that at this combination of frequency and effective field, the FMR main mode is not necessarily excited in the saturated region but instead, a spin wave mode with at least $k_x = 0$ (but not necessarily $k_y = 0$) can be excited (i.e., a backward volume spin wave mode). This result still agrees with the perspective of a 'confined mode' *in the x direction*, since the model becomes a loose approximation to a scenario where domains or saturated regions are present. In other words, it does not account for modes that may show nonzero wave number in a different direction of propagation, such as the y direction (orthogonal to the original domain wall) although it effectively retrieves the expected zero wave number in the x direction (i.e., the domain wall axis). More interestingly, the model predicts the existence of, conceptually speaking, *evanescent* spin waves below that 'pseudo-FMR' frequency condition. In this paper, our scope is in the region where $n > 0$, but a more detailed analysis of the implications from the model when $n \leqslant 0$ can be found in the Supplemental Material [32].

III. MATERIALS AND NUMERICAL METHODS

To obtain insight into the dynamics, we performed a set of micromagnetic simulations using Mumax3 [46]. We simulated a 'rounded bowtie' shaped patch [see Fig. 3(a)] of 6000 nm length, 80 nm thickness (t), and 2000 nm diameter

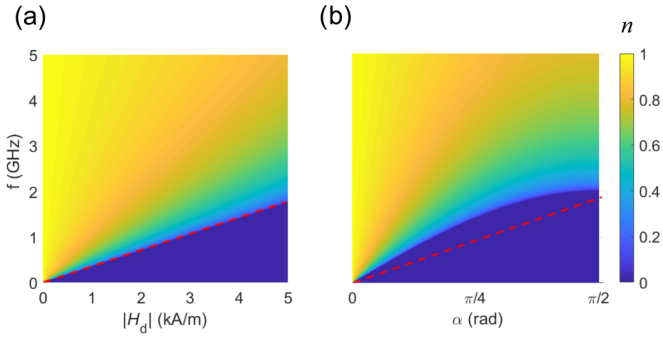

FIG. 2. Contour plots showing the real part of (a) Eq. (13) as a function of the magnitude of the demagnetizing field and (b) Eq. (13) as a function of the angle α for $M_S = 720$ kAm^{-1}, a gyromagnetic ratio $= 2.2\times10^5$ Hz(Am)$^{-1}$ and $A_{ex} = 1.3\times10^{-11}$ Jm^{-1}. Red dashed line with slope γ shows the '$n = 0$' condition in (a). Dark blue area is the imaginary index.

(d) of the circumscribed circles at the ends, with the typical material parameters of Permalloy at room temperature with saturation magnetization $M_s = 7.2\times10^5$ Am^{-1}, exchange constant $A_{ex} = 1.3\times10^{-11}$ Jm^{-1}, and Gilbert damping constant $\alpha_G = 0.008$ for a weighted average of iron and nickel. In the model, the grid was discretized in the x, y, z space into $1536\times512\times16$ cells. The cell size along x and y was 3.9 nm, while the cell size along z was fixed to 4 nm. The cell size along three dimensions is always kept smaller than the exchange length of permalloy (5.3 nm). The number of cells was chosen to be powers of 2 for sake of computational efficiency. We also set a 'smooth edges' condition with value 8. A key point in micromagnetic simulations is to achieve a stable equilibrium magnetization state. We first set a double vortex state with polarity and 'vorticity' numbers of (1,−1) and (1,+1) and then executed the simulation with a high damping ($\alpha_G = 1$) to relax the magnetization until the maximum torque ('maxtorque' parameter in Mumax3), which describes the maximum torque/γ over all cells, where γ is the gyromagnetic ratio of the material, reached 10^{-7} T, indicating convergence and the achievement of a magnetization equilibrium state. The typical time to achieve the equilibrium state was 100 ns. Note that this value has no direct physical meaning due to the artificial high damping. Once the ground state was obtained, damping was set back to original ($\alpha_G = 0.008$), the relaxation process was repeated, the spin configuration was recorded as the ground state of the sample, and then used for the simulations with the dynamic activation. For analyzing time evolution of the magnetic signal, we apply a continuous wave excitation with a magnetic field B at a specific frequency f_0 in the first vortex core region only,

$$B(t) = B_0 \sin(2\pi f_0 t)), \tag{14}$$

and each mode is excited with a relatively small oscillating field, $B_0 = 0.3$ mT. A sampling period of $T_s = 25$ ps was used, recording up to 300 simulated snapshots in space and time, only after the steady state is reached. With these parameters, the time window of observation of the spin waves propagating in the domain wall covers up to 7.5 ns.

To numerically validate the change in wavelength predicted by the model, we run micromagnetic simulations with

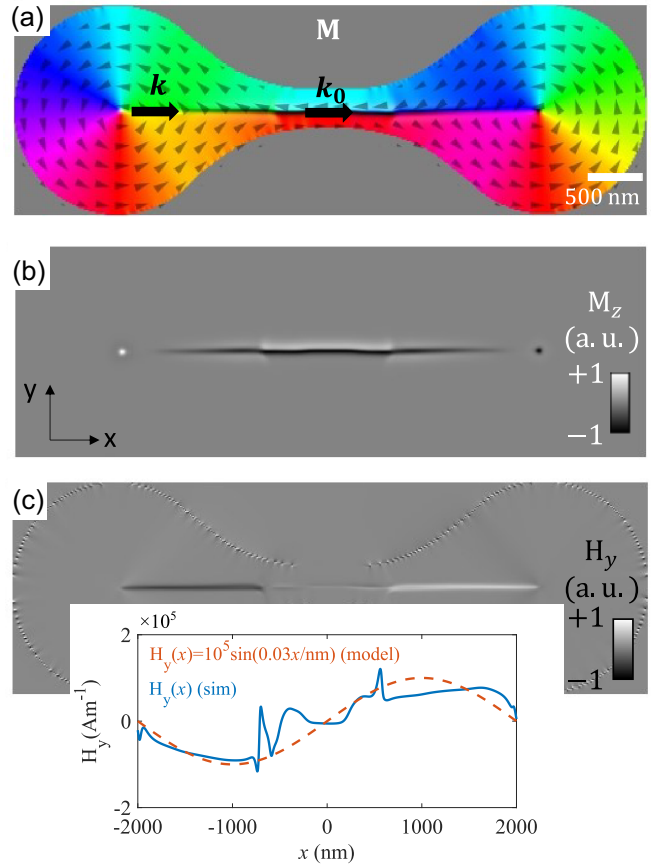

FIG. 3. (a) Schematic of the proposed structure of size 2000 nm×6000 nm×80 nm. A Bloch domain wall is induced and then left to relax before running the dynamic excitations. (b) Normalized out-of-plane component of magnetization is shown, demonstrating the formation of a Bloch domain wall in the middle of the structure. (c) Normalized in-plane y component of the demagnetizing field, showing a reduction in magnitude at the center of the structure. Inset in (c) shows the magnitude of the in-plane component of the demagnetizing field, perpendicular to the wall [$H_y(x)$], along the midwidth of the wall ($y = 0$) obtained from micromagnetic simulations (blue curve) and a sinusoidal dependence with the x position between the two vortex core positions (at $x = 2000$ nm and $x = -2000$ nm from the center of the structure). These are in qualitative good agreement with the proposed 'sinelike' model from Eq. (11). The spatial frequency of 0.03 nm^{-1} is obtained from the slope of the spatially-dependent angle α between magnetic moments in the shape [Fig. 4(a)] (the degree unit can be dropped for simplicity).

an excitation frequency of 1.5 GHz and 3 GHz so Winter's magnons [13] can be efficiently launched from the core region and travel along the domain wall [25]. Numerical results for the spatially dependent wavelength [$\lambda(x)$] are obtained from the time-averaged spectrograms of the channelled spin wave profiles using a Hanning window of 128 FFT points and 100 overlapping points. Since the spatial wavelength is constantly changing along the domain wall length, a fixed width of the window will introduce a tradeoff between spatial frequency resolution and position accuracy in the x direction. A wider spatial window yields less position accuracy to the wave number and a very narrow window cannot properly resolve the spatial frequency at large wavelengths, leading to spatial

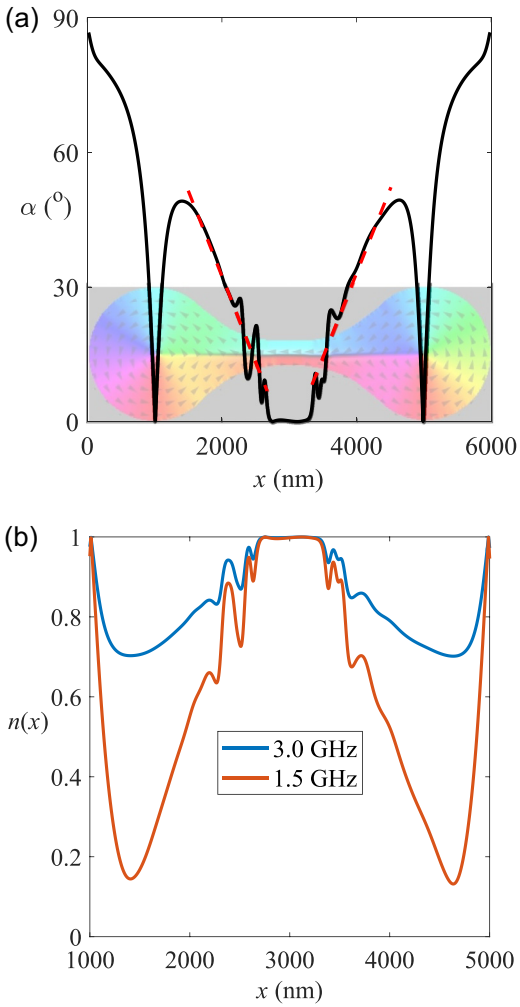

FIG. 4. (a) Profile of angle α for the structure studied in this paper, calculated as $\tan^{-1}(m_y/m_x)$ along a line, parallel to the wall, at 50 nm from the domain wall midwidth. The red dotted line is a linear fit to the values from the vortex core region to the center of the structure. (b) The local mode index from Eq. (13) with the wavelength of a Winter's magnon in a 180 degrees Bloch wall as reference for 3 GHz and 1.5 GHz.

frequency leakage per frequency bin. The chosen parameters of window width and overlapping points are obtained after an optimization process considering several different outcomes. Another solution could be using a width-variable window as described in Ref. [47].

IV. NUMERICAL VALIDATION

In order to validate our model for the real values obtained from Eq. (13), micromagnetic simulations on the magnetic structure shown in Fig. 3(a) are performed and recorded for comparison with the analytical model. Since it is inevitable to start from an angle of approximately $\pi/4$ at the source (the vortex core), the shape of this structure has been chosen so because it allows it to cover the widest range of values of α and therefore of n, see Fig. 4. In this way, for the shape of this patch, the demagnetizing field transversal to the wall is not constant along its length: The angle α at both sides of the wall changes from $\pi/4$ at the core region to 0 at the center of the shape and to $\pi/4$ back again.

Notice that, as reference, a mode index of unity midway between the vortex cores, in a 180 degrees Bloch wall, is considered. The reference wave number k_0 is that of a Winter's magnon along a 180 Bloch wall. For a spin wave propagating from one of the core regions, a reduction in α [or equivalently, a reduction in the transverse demagnetizing field, see Fig. 3(c)] implies an increase in the local wave number. From numerical results on this particular shape, small and smooth variations of the angle are considered far from the core regions, so the assumption $\frac{d\alpha}{dx} \approx 0$ and $\frac{d\Delta_0}{dx} \approx 0$ is still valid and therefore: $\frac{dm}{dy} \approx \frac{dm_y}{dy}$. Close to the core regions, the domain wall angle is large enough to assume the domain wall Neel component to be clearly dominant [40] and therefore, $\frac{dm}{dy} \approx \frac{dm_y}{dy}$ is also satisfied at the center of the domain wall. In other words, the assumptions discussed in the previous section are still valid as well as the model derived for the demagnetizing field transverse to the wall.

Figure 4(a) shows the spatial position profile of angle α from an axis parallel to the domain wall at 50 nm from the center of the wall, calculated as $\tan^{-1}(m_y/m_x)$, where the components of magnetization are extracted from numerical simulations and magnetization is assumed in-plane. The features in the data close to the central region come from the resulting magnetization configuration after a process of relaxation. In that region, the edge with the greatest radius of curvature is closest to the domain wall [see Fig. 4(a)], and the in-plane magnetization keep an apparent 'zigzagging' path as a middle-ground solution to minimize energy. Consequently, as the angle α is calculated from the simulated values of m_x and m_y, the angle local value is also affected. Ideally, this should not be happening, and magnetization should be lying completely in-plane and smoothly following the shape contour even when close to the domain wall. Still, the shape of the structure allows us to approximate the dependence of angle with position x by a fitting linear dependence $\alpha(x) - 0.029x + 87$, see red dotted line in Fig. 4(a). This linear fitting suggests a 'spatial frequency' of $\sim$0.03 nm^{-1} [the degree unit is dropped for simplicity as it is not an official metric (SI) dimension]. The latter result, combined with the proposed model for the demagnetizing field [Eq. (11)] shows good qualitative agreement with the values obtained from simulations [see inset in Fig. 3(c)].

Quantitatively, the simulation result fits better to a sinusoidal function with a maximum value of 10^5 Am^{-1}. While of the same order of magnitude, this value is about three times the maximum of that obtained from the model from Eq. (11) for $\alpha = \pi/4$, which yields a value of $M_s \sin(\pi/4)/4\pi \approx 0.32\times10^5$ Am^{-1} (for a saturation magnetization of 7.2×10^5 Am^{-1}). This quantitative mismatch can be explained by the neglection of other components of the magnetostatic potential in the model, which leads to a 'weaker' demagnetizing field than in reality, due to fewer contributions. We note that these additional contributions should be accounted for a more accurate description.

Figure 4(b) shows the analytical mode index from Eq. (13) with the obtained values of α as inputs for the excitation frequencies of 1.5 GHz and 3 GHz. This agrees with analytical

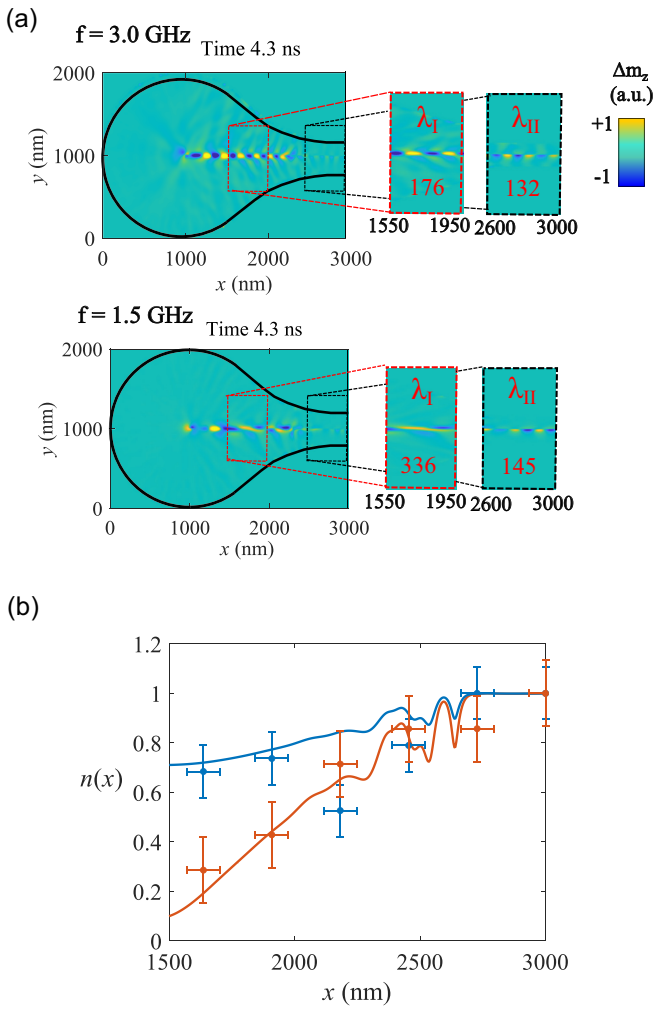

FIG. 5. (a) Simulated wave profiles for an excitation frequency of 3 GHz and 1.5 GHz, with the chosen regions highlighted in dashed lines (note: this does not represent the Hanning window): Region I centered around $x = 1900$ nm and region II centered around $x = 2800$ nm, showing the spin wave profile in one half of the structure. Note that, for ease of comparison, the color scale in the insets for region II is not comparable (it is reduced) to that of region I. The local wavelengths are indicated in the insets, along a length of 400 nm. (b) Results from the analytical model from Eq. (13) (solid curves) for 1.5 GHz (orange) and 3 GHz (blue) and the ratios $\lambda_{II}/\lambda(x)$ obtained from micromagnetic simulations (dots) for each frequency and per Hanning window.

results from Fig. 2(b), at 3 GHz excitation frequency, which show that the wave vector can be reduced as much as approximately 0.7 times the reference wave vector k_0 (i.e., n ≈ 0.7) when the spin wave approaches the core regions (at 900 nm from the vortex core) and α is approximately $\pi/4.8 \approx 0.205\pi$ radians [i.e., 37 degrees, see Fig. 4(a)].

Figure 5(a) shows the wave profile of the propagating mode and the respective wavelengths found in the regions I (λ_I) and II (λ_{II}) (insets). A significant attenuation of the spin wave is observed in region II (the color intensity in the insets is manually adjusted for ease of comparison). We believe this is associated with the 'zigzagging' path of magnetization in the domains that induces a pronounced gradient in the local demagnetizing field halfway between the two regions [see blue curve in the inset of Fig. 3(c)]. In turn, this modifies the spatially local ferromagnetic resonance *in the wall* and thus leads to low transmission between regions in the wall [48,49], as a 1D analogy of the 2D scenario explored in Ref. [49]. Figure 5(b) shows the mode index profiles for 1.5 GHz and 3 GHz (solid lines) obtained from Eq. (13), with the range of angles found from simulations as the input, and numerical results (dots) for the spatial frequency in the x direction, normalized to the value at 3000 nm (i.e., the simulated spatial mode index). Numerical results confirm what the equation predicted: The change in wave number is more pronounced, and more sensitive to the transverse demagnetizing field (or equivalently, to the domain angle α), when the frequency is smaller. Therefore, the range of values for the local mode index is wider at lower frequencies. Also, as expected from the model, the values of the obtained mode index from simulations agree with the predicted values from Eq. (13) with the specified angle $\alpha = 37$ degrees at the corresponding position ($x = 1900$ nm) in the shape ($n \approx 0.7$ at 3 GHz and $n \approx 0.4$ at 1.5 GHz). An apparent physical anomaly for an excitation frequency of 3 GHz is observed from simulations [blue dots in Fig. 5(b)] halfway between the regions I and II, i.e., around $x = 2200$ nm. The x positions near that value actually correspond to the region where the 'zigzagging' of in-plane magnetization is more marked, or in other words, where the edge with the greatest radius of curvature is closest to the domain wall. This suggests that the simulated value is not comparable to the value from the model, which assumes a smooth variation of the demagnetizing field. This may contribute to the considerable mismatch at around $x = 2200$ nm in Fig. 5(b). More importantly, it suggests that the effects of curved edges on propagation in a straight domain wall might be difficult to avoid in certain localized areas in a finite structure and that these are more significant for higher excitation frequencies.

In conclusion, Eq. (12) or its generic form Eq. (4) is proposed as a valid model for finding the local wave number [and Eq. (13) for the local mode index] of a spin wave along domain walls under the influence of different demagnetizing fields or shape contour effects. The model helps to predict how these effects modify the wavelength of a confined mode in a domain wall.

V. SUMMARY

The main result of this work is the proposed mathematical model for an effective spatial frequency dependence of confined spin waves in an 'intermediate angle' domain wall as a function of that angle. The equation of the model is derived from the fundamental Bloch equations of motion, based on an approximate (under reasonable assumptions, similar to those in Ref. [45]) expression of the demagnetizing field transversal to the wall that is applied to a variety of magnonic scenarios. The model can be applied to straight domain walls of variable domain angles, which can be useful as a first approximation to the study of more complex scenarios, such as spin waves in confined structures of arbitrary shapes showing magnetic domains. Reciprocally, the connection between the shape of the magnetic 'patch' and the shape-induced demagnetizing field transverse to the wall potentially allows

us to design a shape for a particularly desired channelled spin wave profile.

The model also leads to situations that have physical meaning such as when considering the FMR main mode frequency or backward volume spin waves propagation in domains, and therefore potentially further extending the applicability of the model to not only localized modes in domain walls.

In summary, an equation for a spatial-dependent wave number for spin waves is proposed, which offers a good model for predicting their propagating behavior in domain walls. This result may help in the development of more complex models for spin wave propagation in nonsaturated nanostructures, spin waves channelled along domain walls, or propagating into magnetic domains.

ACKNOWLEDGMENTS

This work was supported by Engineering and Physical Sciences Research Council (EPSRC) and the Centre of Doctoral Training (CDT) Grant No. EP/L015331/1 in Metamaterials, University of Exeter. All data created during this research are openly available from the University of Exeter's institutional repository [50].

[1] V. V. Kruglyak, S. O. Demokritov, and D. Grundler, J. Phys. D **43**, 264001 (2010).
[2] A. D. Karenowska, A. V. Chumak, A. A. Serga, and B. Hillebrands, in *Handbook of Spintronics*, edited by Y. Xu, D. D. Awschalom, and J. Nitta (Springer, Netherlands, Dordrecht, 2016), pp. 1505–1549.
[3] A. Hoffmann and S. D. Bader, Phys. Rev. Appl. **4**, 047001 (2015).
[4] S. Wintz, V. Tiberkevich, M. Weigand, J. Raabe, J. Lindner, A. Erbe, A. Slavin, and J. Fassbender, Nat. Nanotechnol. **11**, 948 (2016).
[5] G. Dieterle, J. Förster, H. Stoll, A. S. Semisalova, S. Finizio, A. Gangwar, M. Weigand, M. Noske, M. Fähnle, I. Bykova, J. Gräfe, D. A. Bozhko, H. Y. Musiienko-Shmarova, V. Tiberkevich, A. N. Slavin, C. H. Back, J. Raabe, G. Schütz, and S. Wintz, Phys. Rev. Lett. **122**, 117202 (2019).
[6] V. Sluka, T. Schneider, R. Gallardo, A. Kakay, M. Weigand, T. Warnatz, R. Mattheis, A. Roldán-Molina, P. Landeros, V. Tiberkevich, A. Slavin, A. Erbe, A. Deac, J. Lindner, J. Raabe, J. Fassbender, and S. Wintz, Nat. Nanotechnol. **14**, 328 (2019).
[7] C. S. Davies, A. Francis, A. V. Sadovnikov, S. V. Chertopalov, M. T. Bryan, S. V. Grishin, D. A. Allwood, Y. P. Sharaevskii, S. A. Nikitov, and V. V. Kruglyak, Phys. Rev. B **92**, 020408(R) (2015).
[8] C. S. Davies, V. D. Poimanov, and V. V. Kruglyak, Phys. Rev. B **96**, 094430 (2017).
[9] F. B. Mushenok, R. Dost, C. S. Davies, D. A. Allwood, B. J. Inkson, G. Hrkac, and V. V. Kruglyak, Appl. Phys. Lett. **111**, 042404 (2017).
[10] F. G. Aliev, A. A. Awad, D. Dieleman, A. Lara, V. Metlushko, and K. Y. Guslienko, Phys. Rev. B **84**, 144406 (2011).
[11] A. J. Lara, J. R. Moreno, K. Y. Guslienko, and F. G. Aliev, Sci. Rep. **7**, 5597 (2017).
[12] J. M. Winter, Phys. Rev. **124**, 452 (1961).
[13] N. J. Whitehead, S. A. R. Horsley, T. G. Philbin, A. N. Kuchko, and V. V. Kruglyak, Phys. Rev. B **96**, 064415 (2017).
[14] L. Kang, Q. Zhao, H. Zhao, and J. Zhou, Opt. Express **16**, 8825 (2008).
[15] A. B. Rinkevich, D. V. Perov, S. O. Demokritov, M. I. Samoylovich, and O. V. Nemytova, Photon. Nanostruct.: Fundam. Applic. **15**, 59 (2015).
[16] J. B. Pendry, Phys. Rev. Lett. **85**, 3966 (2000).
[17] J.-N. Toedt, M. Mundkowski, D. Heitmann, S. Mendach, and W. Hansen, Sci. Rep. **6**, 33169 (2016).
[18] N. J. Whitehead, S. A. R. Horsley, T. G. Philbin, and V. V. Kruglyak, Phys. Rev. B **100**, 094404 (2019).
[19] N. J. Whitehead, S. A. R. Horsley, T. G. Philbin, and V. V. Kruglyak, Appl. Phys. Lett. **113**, 212404 (2018).
[20] S. Hamalainen, M. Madami, H. Qin, G. Gubbiotti, and S. Dijken, Nat. Commun. **9**, 4853 (2018).
[21] E. Albisetti, D. Petti, G. Sala, R. Silvani, S. Tacchi, S. Finizio, S. Wintz, A. Calò, X. Zheng, J. Raabe, E. Riedo, and R. Bertacco, Commun. Phys. **1**, 56 (2018).
[22] K. Wagner, A. Kákay, K. Schultheiss, A. Henschke, T. Sebastian, and H. Schultheiss, Nat. Nanotechnol. **11**, 432 (2016).
[23] C. Bayer, H. Schultheiss, B. Hillebrands, and R. L. Stamps, IEEE Trans. Magn. **41**, 3094 (2005).
[24] X. S. Wang and X. R. Wang, arXiv:1512.05965.
[25] F. Garcia-Sanchez, P. Borys, R. Soucaille, J.-P. Adam, R. L. Stamps, and J.-V. Kim, Phys. Rev. Lett. **114**, 247206 (2015).
[26] Y. Henry, D. Stoeffler, J.-V. Kim, and M. Bailleul, Phys. Rev. B **100**, 024416 (2019).
[27] E. Schlömann, J. Appl. Phys. **35**, 159 (1964).
[28] D. D. Stancil and F. R. Morgenthaler, J. Appl. Phys. **54**, 1613 (1983).
[29] K. R. Smith, M. J. Kabatek, P. Krivosik, and M. Wu, J. Appl. Phys. **104**, 043911 (2008).
[30] V. E. Demidov, M. P. Kostylev, K. Rott, J. Münchenberger, G. Reiss, and S. O. Demokritov, Appl. Phys. Lett. **99**, 082507 (2011).
[31] P. E. Zilberman, A. G. Temiryazev, and M. P. Tikhomirova, J. Exp. Theor. Phys. **81**, 151 (1995).
[32] See Supplemental Material at http://link.aps.org/supplemental/10.1103/PhysRevB.102.224431 for more details in the corresponding section.
[33] A. Gurevich and G. Melkov, *Magnetization Oscillations and Waves* (CRC Press, Boca Raton, Florida, 1996).
[34] J. C. Slonczewski, J. Appl. Phys. **44**, 1759 (1973).
[35] A. Aharoni, J. Appl. Phys. **83**, 3432 (1998).
[36] L. Landau and E. Lifshitz, Phys. Zeitsch. Sow. **8**, 153 (1935).
[37] A. Hubert and R. Schäfer, *Magnetic Domains: The Analysis of Magnetic Microstructures* (Springer-Verlag, Berlin, Heidelberg, 1998).

[38] D. D. Stancil and A. Prabhakar, *Spin Waves: Theory and Applications* (Springer, Boston, 2009).
[39] E. J. Torok, A. L. Olson, and H. N. Oredson, J. Appl. Phys. **36**, 1394 (1965).
[40] A. L. Olson, H. N. Oredson, E. J. Torok, and R. A. Spurrier, J. Appl. Phys. **38**, 1349 (1967).
[41] K. L. Metlov, Appl. Phys. Lett. **79**, 2609 (2001).
[42] L. Körber, K. Wagner, A. Kákay, and H. Schultheiss, IEEE Magn. Lett. **8**, 1 (2017).
[43] J. A. Osborn, Phys. Rev. **67**, 351 (1945).
[44] D. Berkov and N. Gorn, Phys. Rev. B **71**, 052403 (2005).
[45] M. D. DeJong and K. L. Livesey, Phys. Rev. B **92**, 214420 (2015).
[46] A. Vansteenkiste, J. Leliaert, M. Dvornik, M. Helsen, F. Garcia-Sanchez, and B. Van Waeyenberge, AIP Adv. **4**, 107133 (2014).
[47] S. Nisar, O. U. Khan, and M. Tariq, Computat. Intellig. Neurosci. **2016**, 6172453 (2016).
[48] X.-G. Wang, G.-H. Guo, G.-F. Zhang, Y.-Z. Nie, and Q.-L. Xia, J. Appl. Phys. **113**, 213904 (2013).
[49] L.-J. Chang, Y.-F. Liu, M.-Y. Kao, L.-Z. Tsai, J.-Z. Liang, and S.-F. Lee, Sci. Rep. **8**, 3910 (2018).
[50] https://ore.exeter.ac.uk/repository/.